

# Numerical investigation of transient heat and mass transfer in a parallel-flow liquid-desiccant absorber

Gerardo Diaz

Received: 9 December 2009 / Accepted: 10 August 2010 / Published online: 22 August 2010  
© The Author(s) 2010. This article is published with open access at Springerlink.com

**Abstract** Liquid desiccant systems have received significant attention as a way to reduce latent loads. Tests of liquid desiccant systems in humid climates have shown significant reductions in energy consumption. As moisture in the air is absorbed at the dehumidifier, the temperature of the liquid desiccant increases due to the addition of heat from the enthalpy of condensation of the water vapor. Thus, the coupled effects of heat and mass transfer are relevant for these applications. A two-dimensional mathematical model of the transient heat and mass transfer for an absorber where a thin film of liquid desiccant flows down its walls and dehumidifies the air in parallel-flow configuration is developed and the dynamics of the modeled system are analyzed.

## List of symbols

|             |  |
|-------------|--|
| $B$         | Depth of the channel (m)   |
| $D$         | Diffusion coefficient ( $\text{m}^2 \text{s}^{-1}$ )                   |
| $\text{Fo}$ | Fourier number   |
| $f_s$       | Height of the channel (m)  |
| $g$         | Acceleration of gravity ( $\text{m s}^{-2}$ )                          |
| $H$         | Channel length (m)   |
| $i_{fg}$    | Enthalpy of condensation ( $\text{J kg}^{-1}$ )                        |
| $k$         | Thermal conductivity ( $\text{W m}^{-1} \text{K}^{-1}$ )               |
| $\text{Le}$ | Lewis number   |
| $\dot{m}$   | Mass flow rate ( $\text{kg s}^{-1}$ )                                  |
| $\dot{m}'$  | Mass flow rate per unit of length ( $\text{kg s}^{-1} \text{m}^{-1}$ ) |

|             |                                  |
|-------------|----------------------------------|
| $\text{Nu}$ | Nusselt number                   |
| $P$         | Pressure (Pa)                    |
| $\text{Pe}$ | Peclet number                    |
| $\text{Pr}$ | Prandtl number                   |
| $\text{Re}$ | Reynolds number                  |
| $\text{Sh}$ | Sherwood number                  |
| $T$         | Temperature ( $^\circ\text{C}$ ) |
| $t$         | Time (s)                         |
| $U$         | Dimensionless velocity           |
| $u$         | Velocity ( $\text{m s}^{-1}$ )   |
| $x$         | Direction along the channel (m)  |
| $y$         | Direction across the channel (m) |

|          |   |
|----------|---|
| $\alpha$ | Thermal diffusivity ( $\text{m}^2 \text{s}^{-1}$ )  |
| $\delta$ | Thickness (m)   |
| $\eta$   | Dimensionless coordinate across the channel   |
| $\mu$    | Dynamic viscosity ( $\text{kg m}^{-1} \text{s}^{-1}$ )  |
| $\nu$    | Kinematic viscosity ( $\text{m}^2 \text{s}^{-1}$ )  |
| $\omega$ | Air humidity ratio ( $\text{kg}_{\text{wv}} \text{kg}_{\text{da}}^{-1}$ )                     |
| $\rho$   | Density ( $\text{kg m}^{-3}$ )  |
| $\tau$   | Time constant (s)   |
| $\theta$ | Dimensionless temperature   |
| $\xi$    | Dimensionless coordinate along the channel  |
| $\zeta$  | Water concentration in liquid desiccant ( $\text{kg}_{\text{water}}/\text{kg}_{\text{sol}}$ ) |

## Greek symbols

|          |   |
|----------|---|
| $\alpha$ | Thermal diffusivity ( $\text{m}^2 \text{s}^{-1}$ )  |
| $\delta$ | Thickness (m)   |
| $\eta$   | Dimensionless coordinate across the channel   |
| $\mu$    | Dynamic viscosity ( $\text{kg m}^{-1} \text{s}^{-1}$ )  |
| $\nu$    | Kinematic viscosity ( $\text{m}^2 \text{s}^{-1}$ )  |
| $\omega$ | Air humidity ratio ( $\text{kg}_{\text{wv}} \text{kg}_{\text{da}}^{-1}$ )                     |
| $\rho$   | Density ( $\text{kg m}^{-3}$ )  |
| $\tau$   | Time constant (s)   |
| $\theta$ | Dimensionless temperature   |
| $\xi$    | Dimensionless coordinate along the channel  |
| $\zeta$  | Water concentration in liquid desiccant ( $\text{kg}_{\text{water}}/\text{kg}_{\text{sol}}$ ) |

## Subscripts and superscripts

|       |             |
|-------|-------------|
| AVG   | Average     |
| $a$   | Air         |
| $d$   | Desiccant   |
| $da$  | Dry air     |
| 0     | Initial     |
| int   | Interface   |
| $sol$ | Solution    |
| $w$   | Wall        |
| $wv$  | Water vapor |

G. Diaz (✉)  
School of Engineering, University of California-Merced,  
5200 North Lake Road, Merced, CA 95343, USA  
e-mail: gdiaz@ucmerced.edu

## 1 Introduction

Liquid desiccants have been proposed as a way to reduce energy consumption by lowering latent loads on evaporators and cooling coils. Numerical and experimental studies have shown improvements in the coefficient of performance of air conditioning systems using liquid desiccants [1, 2]. Other studies have concentrated on the physical aspects of the heat and mass transfer between moist air and liquid desiccant under a variety of geometries and operating conditions. For instance, Park et al. [3] performed a numerical and experimental study of the steady-state coupled heat and mass transfer between a falling desiccant film and air in cross-flow. They considered both regeneration and absorption processes. Khan [4] developed a two dimensional steady state model of an internally cooled liquid desiccant absorber. The total and latent cooling loads compared well against experimental values from commercially available absorber performance. Kessling et al. [5] developed an energy and mass balance model and determined the dominant effects on the absorption process in an energy storage application using a liquid desiccant. Mass transfer coefficients were measured and reported in their work. A detailed steady-state two-dimensional model for cooling and dehumidification of air by a falling film in parallel flow was developed by Rahamah et al. [6]. They found that low air flow rates produced better dehumidification and cooling. More recently, Ali et al. [7] performed a comparative study between parallel and counter flow configurations for heat and mass exchange of humid air and a falling film of liquid desiccant in the presence of nanoparticle suspensions. Their numerical results showed that parallel flow provided better dehumidification and cooling of air than counter flow for a wide range of parameters. Also, it was shown that dehumidification and cooling was enhanced by increasing the volume fraction of nanoparticles and the dispersion factor. In a follow-up paper, the same authors conducted a numerical analysis of heat and mass transfer between air and a falling liquid-desiccant film in cross-flow configuration [8]. In this study, they also considered the effects of adding small Cu-ultrafine particles to the liquid desiccant solution. The results of their work showed that an increase in the height and length of the channel and a decrease in the channel width enhanced the dehumidification and cooling processes. Finally, Ali and Vafai [9] numerically investigated the heat and mass transfer between air and desiccant film in inclined parallel and counter flow channels also considering the presence of Cu-ultrafine particles. Their main findings indicated that inclination played a significant role in improving dehumidification and cooling in both parallel and counter flow channels. They also found that the addition of Cu-ultrafine particles increased the effective thermal conductivity of the

solid–liquid mixture. However, the improvement in dehumidification, cooling, and regeneration due to the presence of the particles was minimal due to the small thickness of the desiccant film. A similar steady-state two-dimensional model was used by Mesquita et al. [10] to study the effect of constant liquid desiccant film thickness compared to using variable film thickness for parallel plate dehumidifiers. Heat and mass transfer correlations as well as finite differences and a simplified one-dimensional model were used to show that the constant thickness under-predicted the dehumidification process at low liquid desiccant rates. Several other authors have developed analytical solutions of steady-state heat and mass transfer between air and liquid desiccant for parallel, counter, or cross flow configurations [11–13].

Considerably less work has been done on transient absorption and regeneration of air using liquid desiccants. Hajji and Worek [14] performed a theoretical analysis of transient combined heat and mass transfer in a stagnant liquid layer absorbing water vapor. Their model considered two different boundary conditions at the lower surface of the film. Analytical expressions for the temperature and concentration profiles were reported. Nakoryakov et al. [15, 16] also analyzed the heat and mass transfer during vapor absorption by a stagnant solution layer. They presented an analytical solution for short and long times. Experimental results of transient heat and mass transfer in liquid desiccant systems are very scarce. Gandhidasan et al. [17] investigated the transient behavior of a gauze-type structured packing liquid desiccant dehumidifier. More recently, Peng and Pan [18] used a local volumetric average approach to develop a transient one-dimensional model of a liquid desiccant process at low flow conditions. The results were compared with the measurements at a experimental test stand filled with plastic pall ring packing material.

Other authors have analyzed transient dehumidification and regeneration using solid desiccants. Tauscher et al. [19] investigated the transient dehumidification of air inside the narrow channels of a rotary solid storage element. In their work, several narrow-channel geometries were investigated experimentally and numerically. Al-Sharqawi and Lior [20] performed a numerical study of transient flow with heat and mass transfer between desiccant plates and humid air. The effects of plate thickness, Reynolds number, and turbulent intensity were analyzed. Their results indicated that 25% higher heat and mass transfer coefficients were obtained increasing the desiccant plate thickness. They reported that mass transfer rates increased with higher Reynolds numbers and turbulent flow augmented the rate of dehumidification.

The analysis of transient thermal performance of parallel, counter, or cross-flow exchangers has dealt mainly with temperature changes over time and response to step changes

of inlet temperatures and mass flow rates [21–23]. However, transient response of temperature, humidity ratio, and liquid desiccant concentration on heat and mass exchangers has not been analyzed in depth. In this paper, a two-dimensional transient model for the analysis of temperature and concentration change over time is developed and applied to the study of heat and mass exchange between humid air and liquid desiccant in a parallel flow configuration. The effect of the wall has been considered for adiabatic and constant temperature boundary conditions.

## 2 Mathematical formulation

The transient governing equations for a liquid desiccant film flowing from top to bottom in parallel with a stream of humid air, as shown in Fig. 1, are described as follows.

### 2.1 Two-dimensional transient model

The velocity profile for the two dimensional model is obtained analytically assuming fully developed laminar flow. From the momentum equation, the velocity profile for the liquid desiccant side is [6]:

$$u_d = \frac{gy_d}{v} \left( \delta_d - \frac{1}{2}y_d \right) \quad (1)$$

The air-side velocity profile can be shown to be

$$u_a = u_d + \frac{1}{2\mu_a} \frac{dP}{dx} (y_a^2 - \delta_a^2) \quad (2)$$

where  $\delta_a = \frac{1}{2}f_s - \delta_d$ . The pressure drop along the channel becomes:

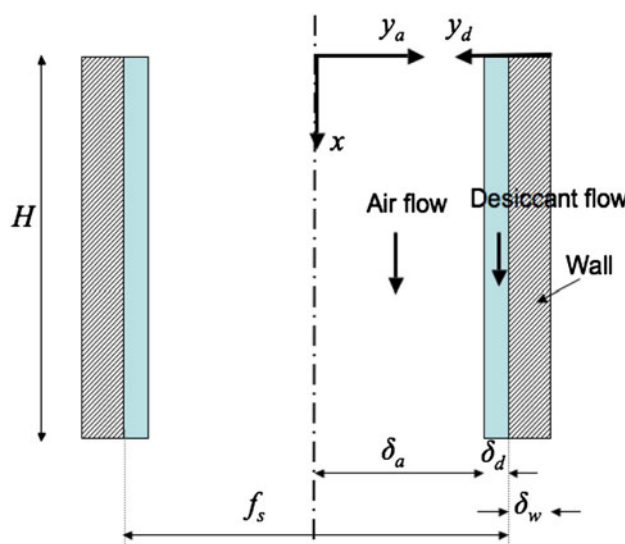


**Fig. 1** Description of the geometry. The depth  $B$  of the channel has been considered of unitary magnitude

$$\frac{dP}{dx} = \frac{3\mu_a u_d}{\delta_a^2} - \frac{3v_a \dot{m}_a}{2\delta_a^3 B} \quad (3)$$

The desiccant film thickness is obtained applying continuity to the cross section of the film

$$\frac{\dot{m}'_d}{2} = \int_0^{\delta_d} \rho_d u_d dy \quad (4)$$

where  $\dot{m}'_d$  is the total mass flow rate of liquid desiccant inside the channel per unit of depth. Thus, the thickness of the film can be expressed as:

$$\delta_d = \left( \frac{3\dot{m}'_d v_d}{2\rho_d g} \right)^{1/3} \quad (5)$$

The governing equations for energy and mass transfer become:

Air side

$$\frac{\partial T_a}{\partial t} + u_a \frac{\partial T_a}{\partial x} = \alpha_a \frac{\partial^2 T_a}{\partial y_a^2} \quad (6)$$

$$\frac{\partial \omega}{\partial t} + u_a \frac{\partial \omega}{\partial x} = \mathcal{D}_a \frac{\partial^2 \omega}{\partial y_a^2} \quad (7)$$

Liquid desiccant side

$$\frac{\partial T_d}{\partial t} + u_d \frac{\partial T_d}{\partial x} = \alpha_d \frac{\partial^2 T_d}{\partial y_d^2} \quad (8)$$

$$\frac{\partial \zeta}{\partial t} + u_d \frac{\partial \zeta}{\partial x} = \mathcal{D}_d \frac{\partial^2 \zeta}{\partial y_d^2} \quad (9)$$

Wall

$$\frac{\partial T_w}{\partial t} = \alpha_w \frac{\partial^2 T_w}{\partial y_d^2} \quad (10)$$

Air–liquid desiccant interface

$$-\left[ k_a \frac{\partial T_a}{\partial y_a} + \rho_a \mathcal{D}_a i_{fg} \frac{\partial \omega}{\partial y_a} \right] \Big|_{y_a=\delta_a} = k_d \frac{\partial T_d}{\partial y_d} \Big|_{y_d=\delta_w+\delta_d} \quad (11)$$

$$-\rho_a \mathcal{D}_a \frac{\partial \omega}{\partial y_a} \Big|_{y_a=\delta_a} = \rho_d \mathcal{D}_d \frac{\partial \zeta}{\partial y_d} \Big|_{y_d=\delta_w+\delta_d} \quad (12)$$

Liquid desiccant–wall interface

$$k_d \frac{\partial T_d}{\partial y_d} \Big|_{y_d=\delta_w} = k_w \frac{\partial T_w}{\partial y_d} \Big|_{y_d=\delta_w} \quad (13)$$

The set of equations is completed with the relations for equilibrium of the air humidity ratio with the liquid desiccant water concentration [8]. The interfacial humidity ratio is obtained as

$$\omega_{int} = 0.62185 \frac{P_z}{P_t - P_z} \quad (14)$$

where the vapor pressure for Calcium Chloride liquid desiccant is obtained with

$$P_z = P_{wv} \left( 1 - 0.828Z - 1.496Z^2 + Z \frac{T_{\text{int}} - 40}{350} \right) \quad (15)$$

where  $P_{wv}$  is the partial pressure of water vapor in humid air and  $Z = 1 - \zeta_{\text{int}}$ .

#### Initial and boundary conditions

The initial conditions correspond to

$$T_a = T_a^0, \omega = \omega^0, T_d = T_d^0, \zeta = \zeta^0, T_w = T_w^0, \quad (16)$$

and the boundary conditions are as follows.

$$x = 0 : T_a = T_a^0, \omega = \omega^0, T_d = T_d^0, \zeta = \zeta^0 \quad (17)$$

$$y_a = 0 : \frac{\partial u_a}{\partial y_a} = 0, \frac{\partial T_a}{\partial y_a} = 0, \frac{\partial \omega}{\partial y_a} = 0 \quad (18)$$

$$y_d = 0 : \frac{\partial T_w}{\partial y_d} = 0 \quad (19)$$

$$y_d = \delta_w : u_d = 0, T_d = T_w, \frac{\partial \zeta}{\partial y_d} = 0 \quad (20)$$

$$y_a = \delta_a : u_a = u_d, \omega = \omega_{\text{int}} \quad (21)$$

$$y_d = \delta_w + \delta_d : \frac{\partial u_d}{\partial y_d} = 0, T_d = T_a \quad (22)$$

#### 2.1.1 Nondimensional formulation

Using the nondimensional parameters  $\xi = x/f_s$ ,  $\eta_a = y_a/f_s$ ,  $\eta_d = y_d/f_s$ ,  $U_a = u_a/u_{a_{\max}}$ ,  $U_d = u_d/u_{d_{\max}}$ ,  $\theta = (T - T_w^0)/(T_a^0 - T_w^0)$ , and  $\text{Fo} = t/\tau_a$ , the dimensionless representation of the governing equations takes the form:

#### Air side

$$\frac{\partial \theta_a}{\partial \text{Fo}} + \text{Pe}_a U_a \frac{\partial \theta_a}{\partial \xi} = \frac{\partial^2 \theta_a}{\partial \eta_a^2} \quad (23)$$

$$\frac{\partial \omega}{\partial \text{Fo}} + \text{Pe}_a U_a \frac{\partial \omega}{\partial \xi} = \frac{1}{\text{Le}_a} \frac{\partial^2 \omega}{\partial \eta_a^2} \quad (24)$$

#### Liquid desiccant side

$$\frac{\partial \theta_d}{\partial \text{Fo}} + \text{Pe}_d \Gamma_1 U_d \frac{\partial \theta_d}{\partial \xi} = \Gamma_1 \frac{\partial^2 \theta_d}{\partial \eta_d^2} \quad (25)$$

$$\frac{\partial \zeta}{\partial \text{Fo}} + \text{Pe}_d \Gamma_1 U_d \frac{\partial \zeta}{\partial \xi} = \frac{1}{\text{Le}_d} \Gamma_1 \frac{\partial^2 \zeta}{\partial \eta_d^2} \quad (26)$$

#### Wall

$$\frac{\partial \theta_w}{\partial \text{Fo}} = \Gamma_2 \frac{\partial^2 \theta_w}{\partial \eta_d^2} \quad (27)$$

where  $\tau_a = f_s^2/\alpha_a$ ,  $\text{Le}_a = \alpha_a/\mathcal{D}_a$ ,  $\text{Pe}_a = \text{Re}_a \text{Pr}_a$ ,  $\text{Le}_d = \alpha_d/\mathcal{D}_d$ ,  $\text{Pe}_d = \text{Re}_d \text{Pr}_d$ ,  $\Gamma_1 = \alpha_d/\alpha_a$  and  $\Gamma_2 = \alpha_w/\alpha_a$ .

### 3 Method of solution

An implicit finite difference scheme is used to solve the set of equations for the two-dimensional transient model. Upwind and central differences are used for first and second order derivatives in space, respectively. Equations 11 and 12 are solved to obtain the temperature and concentration of water in the liquid desiccant at the interface. Then, Eqs. 14 and 15 are solved to obtain the humidity ratio,  $\omega_{\text{int}}$ . This information is used to solve the governing equations for the air and liquid-desiccant sides. The algorithm iterates at each time step until it converges to an arbitrary tolerance level.

The model and method of solution were validated using the most closely related test data found in the literature. The model was modified to run a counterflow structured packing liquid desiccant dehumidifier. The operating conditions and geometric parameters were obtained based on the information provided in [17]. The inlet air temperature and relative humidity were 26°C and 66.35%, respectively. Figure 2a and b show the comparison with the experimental values obtained by Gandhidasan et al. [17]. Good agreement is obtained with the model under-predicting the steady state value of the temperature by 1.5°C and the over-predicting the relative humidity by 4.9%. The transient behavior predicted by the model matched the experimental results.

### 4 Results and discussion

The developed model is used to predict the behavior of a liquid desiccant film in contact with humid air in parallel flow inside a channel.

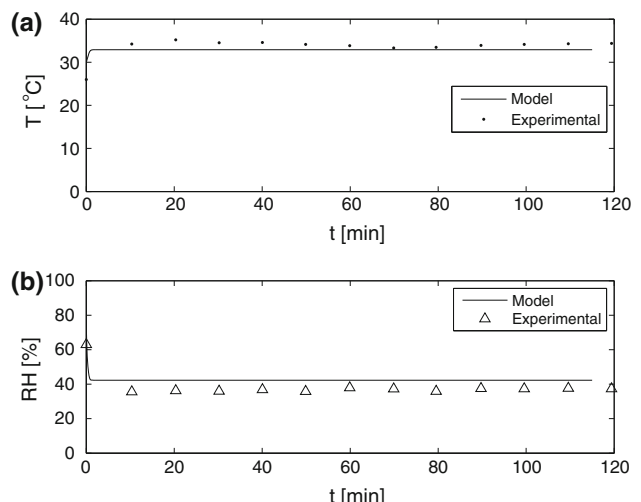


**Fig. 2** Comparison of variation of air outlet temperature and relative humidity with time. **a** Outlet temperature, **b** relative humidity. Experimental values obtained from [17]

#### 4.1 Temperature and water concentration variation over time

The variation of temperature and water concentration in the air and liquid desiccant domains as a function of time for a channel of length  $H = 0.4$  m is analyzed in this section. The operating parameters used for the simulations are described in Table 1. Figure 3a–c show the average outlet conditions at  $\xi = H/f_s$  for the humid air and liquid desiccant. The wall temperature at the outlet location is also displayed. At  $Fo = 0$  there is a uniform distribution of temperature and water content at each domain. As  $Fo$  increases there is a rapid cooling of the air and liquid desiccant mainly due to the effect of the low initial temperature of the wall. This is followed by a smooth increase in the temperatures of the air and liquid desiccant,  $\theta_a$  and  $\theta_d$ , respectively, as seen in Fig. 3a. The temperatures stabilize at  $Fo = 30$ , approximately. The air humidity ratio, shown in Fig. 3b, shows a similar overall behavior as  $\theta_a$  having an initial drop in its value followed by a moderate increase to reach steady-state near  $Fo = 30$ . The fraction of water in the liquid desiccant solution, seen in Fig. 3c, shows a different dynamic behavior presenting an overshoot at  $Fo \approx 20$  and then stabilizing at  $Fo$  equal to 35, approximately.

The difference in the dynamic behavior of  $\omega$  and  $\zeta$  can also be observed analyzing the distribution of these variables over time. Figure 4 shows a contour plot of the air humidity distribution at eight different discrete values of  $Fo$ . The interface with the liquid desiccant is located at  $\eta_a = \delta_d/f_s$  and the axis of symmetry of the channel is located at  $\eta_a = 0$ . Air enters the channel with  $\omega = 0.02 \text{ kg}_{\text{wv}}/\text{kg}_{\text{da}}$  at  $\xi = 0$  and the air humidity is absorbed at the interface between air and liquid desiccant. Therefore, the humidity ratio decreases as  $\eta_a$  increases. At very short

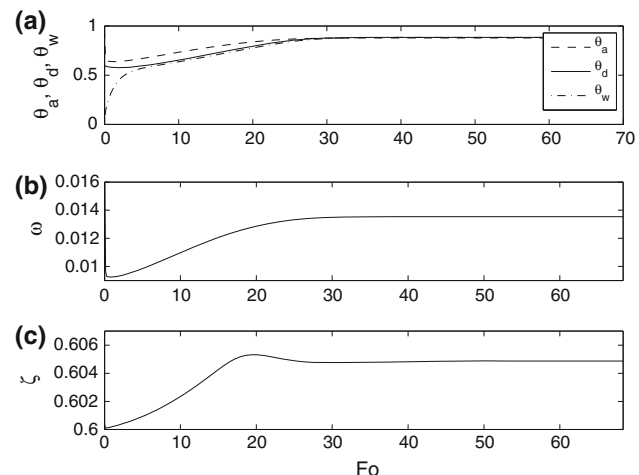


**Fig. 3** Outlet average conditions for transient behavior in parallel flow. **a** dashed line  $\theta_a$ , solid line  $\theta_d$ , dash-dotted line  $\theta_w$ ; **b**  $\omega$ ; **c**  $\zeta$

times the results show a gradient of  $\omega$  that is approximately parallel to the air/liquid-desiccant interface. As  $Fo$  increases, the results show a decreasing value of  $\omega$  in the positive direction of  $\xi$ . The variation in the distribution of  $\omega$  is less evident as time increases reaching steady-state near  $Fo = 34$ .

The change in the distribution of  $\zeta$  over time is shown in Fig. 5. The same discrete values of  $Fo$  displayed in Fig. 4 were used. The interface with the wall is located at  $\eta_d = \delta_w/f_s$  and the interface with the humid air is located at  $\eta_d = (\delta_d + \delta_w)/f_s$ . The liquid desiccant enters the channel with  $\zeta = 0.6$  at  $\xi = 0$ . At short times, i.e.  $Fo = 0.013669$ , the gradient of water concentration remains parallel to the air/liquid-desiccant interface and the variation is located in the close vicinity of the interface. Iso- $\zeta$  lines are indistinguishable. Faster rates of diffusion are prevented by the low value of  $D_d$ . At larger times, the water concentration in the desiccant increases near the interface showing a variation with respect to the length of the channel that is not as strong as the change in the direction towards the wall. The dynamics are slow compared to other variables reaching steady state conditions near  $Fo = 41$ .

#### 4.2 Effect of boundary condition at the wall

The results presented in the previous sections were obtained by using an adiabatic boundary condition for the wall at  $\eta_d = 0$ . This situation is valid in cases where no cooling is needed for the absorber, such as in refrigerated warehouses applications [24]. However, in many situations, a coolant fluid runs inside the walls of the absorber to remove the heat generated due to water vapor condensation, keeping the wall temperature approximately constant. Thus, the boundary condition at the wall is modified to

**Table 1** Operating parameters and properties used in the analysis [7]

| Parameter (units)   | Desiccant             | Air                   | Wall  |
|---|-----------------------|-----------------------|-------|
| $T_a^0$ (°C)  |                       | 35                    |       |
| $T_d^0$ (°C)  | 25                    |                       |       |
| $\omega^0$ ( $\text{kg}_{\text{wv}}\text{kg}_{\text{da}}^{-1}$ )    |                       | 0.02                  |       |
| $\zeta^0$ ( $\text{kg}_{\text{water}}\text{kg}_{\text{sol}}^{-1}$ ) | 0.6                   |                       |       |
| $\dot{m}_a$ ( $\text{kg s}^{-1}$ )                                  |                       | 0.012395              |       |
| $\dot{m}'_d$ ( $\text{kg s}^{-1}\text{m}^{-1}$ )                    | 0.014                 |                       |       |
| $T_w^0$ (°C)  |                       |                       | 10    |
| $k$ ( $\text{W m}^{-1} \text{K}^{-1}$ )                             | 0.525                 | 0.02635               | 0.026 |
| $C_p$ ( $\text{J kg}^{-1}\text{K}^{-1}$ )                           | 2,330                 | 1,028                 | 500   |
| $\rho$ ( $\text{kg m}^{-3}$ )                                       | 1,394                 | 1.172                 | 146   |
| $\mu$ ( $\text{kg m}^{-1} \text{s}^{-1}$ )                          | $1.19 \times 10^{-2}$ | $1.83 \times 10^{-5}$ |       |
| $D$ ( $\text{m}^2 \text{s}^{-1}$ )                                  | $4.2 \times 10^{-10}$ | $2.5 \times 10^{-5}$  |       |

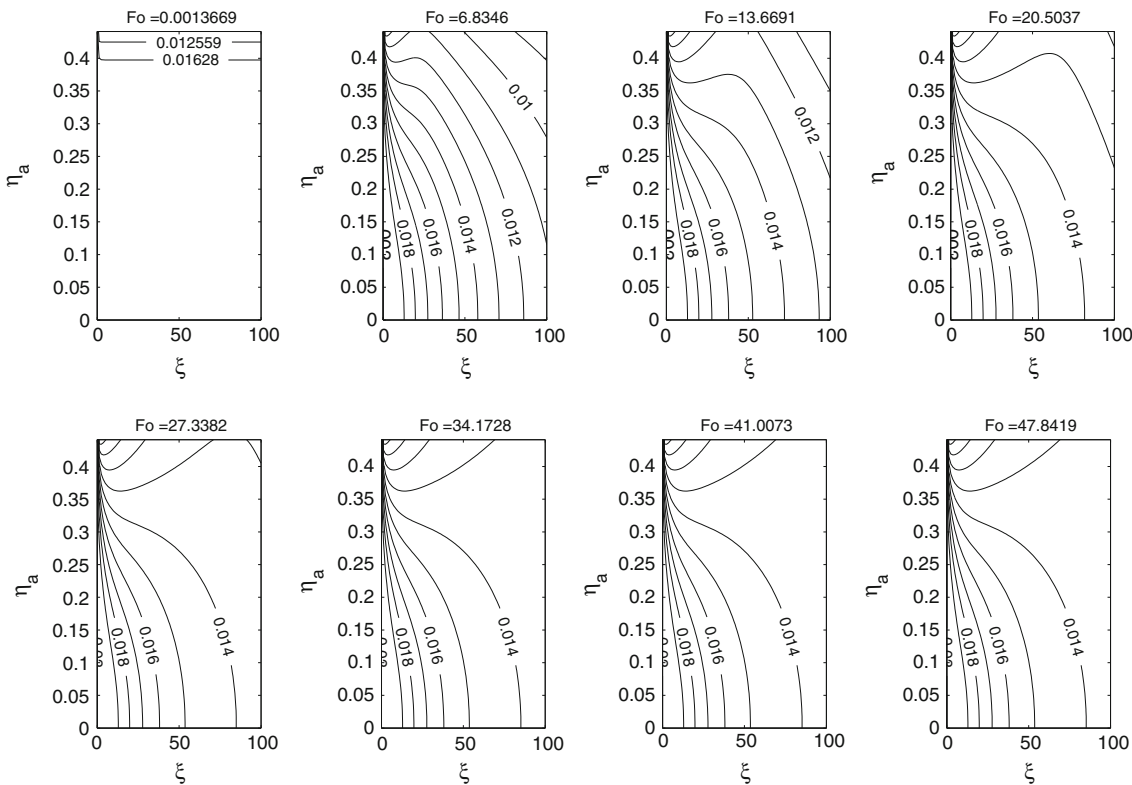


**Fig. 4** Spatial distribution of  $\omega$  as a function of dimensionless time  $Fo$

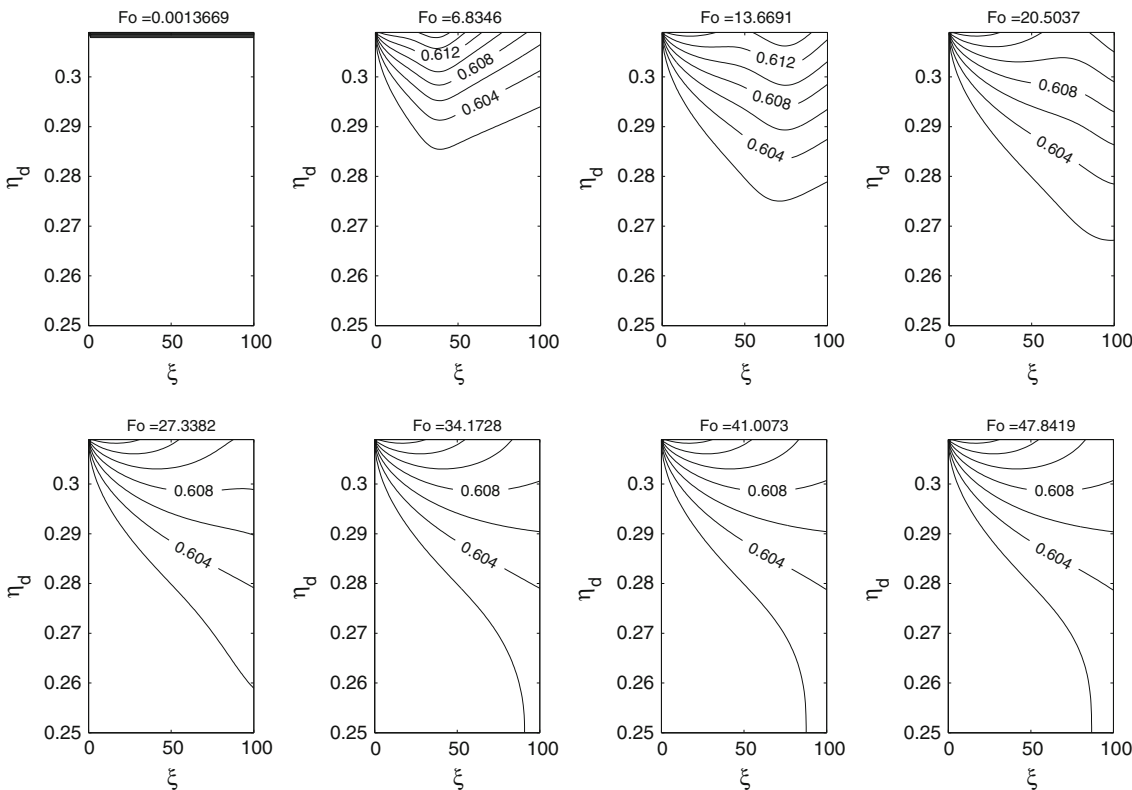


**Fig. 5** Spatial distribution of  $\zeta$  as a function of dimensionless time  $Fo$

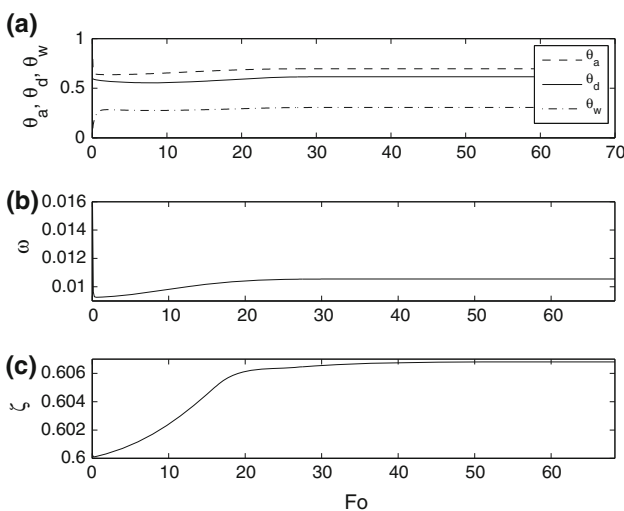


**Fig. 6** Outlet average conditions for transient behavior in parallel flow for constant wall temperature. **a** dashed line  $\theta_a$ , solid line  $\theta_d$ , dash-dotted line  $\theta_w$ ; **b**  $\omega$ ; **c**  $\zeta$

have a constant value equal to  $T_w^0$ . Figure 6 shows the transient behavior of the average values at the outlet of the channel for temperature and water concentrations. It is observed that, at all times, the temperature of the liquid desiccant remains below the temperature of the air. This is caused by the effect of the wall that remains at a lower temperature compared to the other two fluids, absorbing heat at the interface with the liquid desiccant film. The lower liquid desiccant temperature enhances the moisture absorption properties of the liquid desiccant so the outlet air humidity ratio is lower than for the case with adiabatic wall boundary condition. This causes the water content in the liquid desiccant to increase with respect to the adiabatic-wall case. It is also observed that the overshoot seen in Fig. 3 in  $\zeta$  is no longer present.

#### 4.3 Effect of step changes on a single variable

A liquid desiccant heat and mass exchanger is frequently subject to changes in the values of the operating parameters. Ambient air temperature, humidity ratio, liquid desiccant temperature and concentration can vary over time having an effect in the overall performance of the dehumidification process. In this section, the response of the model to variations in a single inlet parameter is analyzed by introducing step changes during the dynamic simulation. Each inlet variable is increased and decreased by an arbitrary 10% and the dynamics of the system subject to these changes are obtained. Transient simulations show that the air humidity ratio and liquid desiccant concentration have the strongest effect on the other variables. These results are presented in the following subsections.

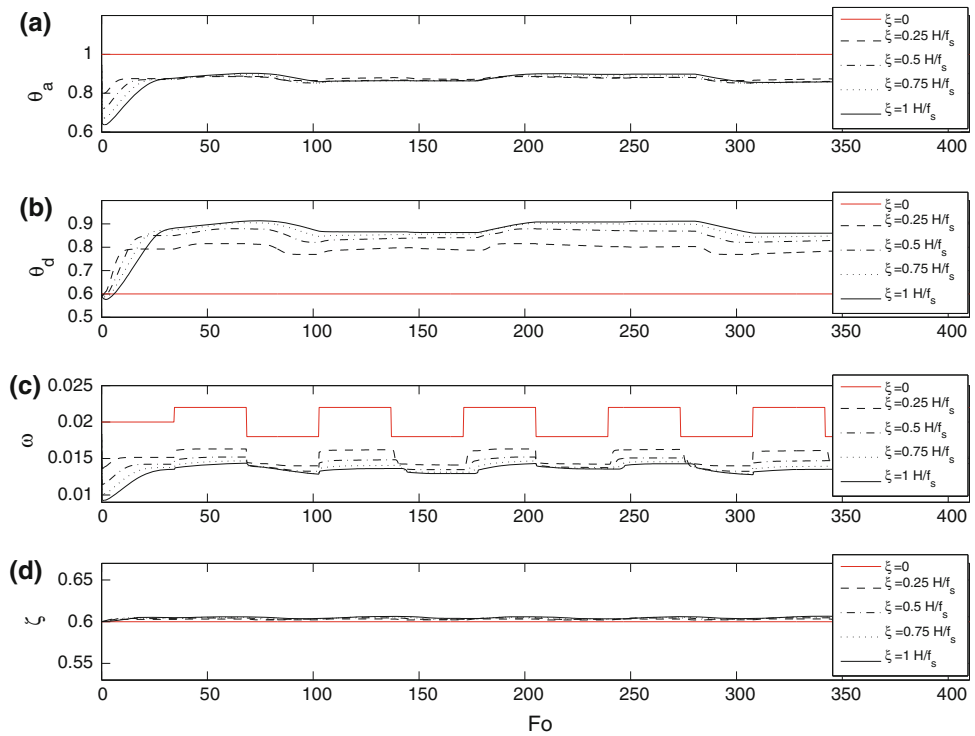
##### 4.3.1 Changes in $\omega(\xi = 0, Fo)$

Figure 7a–d show the effect of the step changes in  $\omega(\xi = 0, Fo)$  on the step changes in  $\theta_a$ ,  $\theta_d$ , and  $\zeta$ . The average value of these variables are plotted at five different locations along the length of the channel, i.e.  $\xi = 0, 0.25 H/f_s, 0.5 H/f_s, 0.75 H/f_s$ , and  $H/f_s$ . Figure 7a shows that the air temperature inside the channel decreases very rapidly in the first quarter of the channel length. The step changes in  $\omega(\xi = 0, Fo)$  produce only a minor change in the value of  $\theta_a$  and a delay is observed in the reaction of the temperature along the length of the channel. It is seen that a lower frequency is obtained in the oscillation of  $\theta_a$  compared to  $\omega$ . Figure 7b shows a more gradual change in the value of  $\theta_d$  with respect to  $\xi$ . The value of  $\theta_d$  at the end of the channel, shown by a solid black line, indicates that the outlet temperature conditions do not differ significantly between the air and liquid desiccant. The lower frequency of oscillation is also observed in this variable. Figure 7c displays the effect of the forcing function introduced in  $\omega(\xi = 0, Fo)$ . The simulation is started with the values indicated in Table 1. Then step changes occur every  $\Delta Fo \approx 34$ . It is observed that the air humidity also decreases significantly in the first quarter of the channel length and the amplitude of oscillation decreases gradually as  $\xi$  increases. A delay in the reaction of  $\omega$  is seen as  $\xi$  increases. The liquid desiccant water concentration  $\zeta$ , depicted in Fig. 7d, is not modified significantly by the changes in  $\omega$  and remains at a value close to 0.6. However, the small increment in  $\zeta$  for larger values of  $\xi$  indicates water absorption from the moist air.

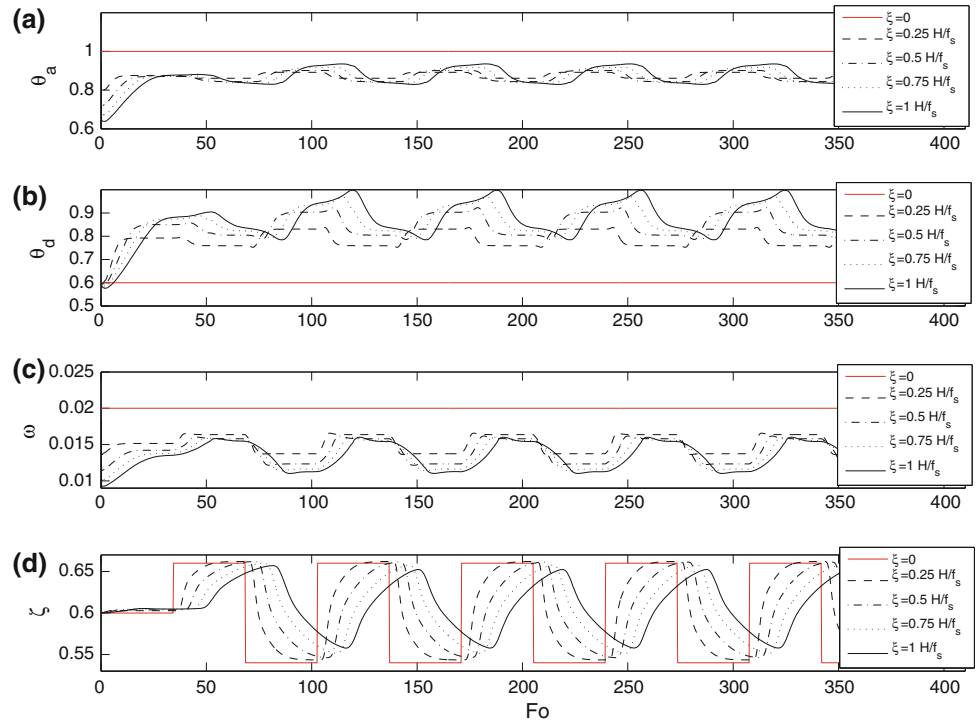
##### 4.3.2 Changes in $\zeta(\xi = 0, Fo)$

A substantial difference in the dynamic behavior is observed when the water content in the liquid desiccant at  $\xi = 0$  is varied using step changes as shown in Fig. 8a–d. Figure 8d clearly displays the delay effect in the variation of  $\zeta$  as a function of  $\xi$ . The concentration of water in the liquid desiccant at different values of  $\xi$  shows a first order system behavior with no signs of overshoot.  $\zeta$  at  $\xi = 0.25 H/f_s$  closely follows the forcing function and it reaches steady state before the next step change. The water concentration at the remaining locations inside the channel shows a delay with respect to the forcing function with a decreasing amplitude of oscillation observed for increasing values of  $\xi$ . Water concentration at  $\xi = 0.5 H/f_s$ ,  $\xi = 0.75 H/f_s$ , and at the end of the channel shows a smaller amplitude of oscillations since the delay effect prevents these locations to reach steady state before the next step change. The effect of the change in  $\zeta$  is clearly observed in the other variables. Figure 8a and b show much larger oscillations in  $\theta_a$  and  $\theta_d$  compared to Fig. 7. In particular, the temperature change in  $\theta_d$  is larger at the end of the channel while the opposite is

**Fig. 7** Effect of step changes in  $\omega(\xi = 0, \text{Fo})$ . **a**  $\theta_a$ ; **b**  $\theta_d$ ; **c**  $\omega$ ; **d**  $\zeta$ . The lines correspond to: solid red line at  $\xi = 0$ , dashed line at  $\xi = 0.25 \text{ H}/f_s$ , dash-dotted line at  $\xi = 0.5 \text{ H}/f_s$ , dotted line at  $\xi = 0.75 \text{ H}/f_s$ , and solid black line at  $\xi = 1 \text{ H}/f_s$



**Fig. 8** Effect of step changes in  $\zeta(\xi = 0, \text{Fo})$ . **a**  $\theta_a$ ; **b**  $\theta_d$ ; **c**  $\omega$ ; **d**  $\zeta$ . The lines correspond to: solid red line at  $\xi = 0$ , dashed line at  $\xi = 0.25 \text{ H}/f_s$ , dash-dotted line at  $\xi = 0.5 \text{ H}/f_s$ , dotted line at  $\xi = 0.75 \text{ H}/f_s$ , and solid black line at  $\xi = 1 \text{ H}/f_s$



true for  $\theta_a$ . Finally, Fig. 8c shows that a reduction in  $\zeta$  implies a more concentrated liquid desiccant solution and thus it absorbs more humidity from the air, lowering the value of  $\omega$ . However, there is a small delay in the reduction of  $\omega$  as a response to a reduction in  $\zeta$ . The inverse effect is also observed when the value of  $\zeta$  is increased.

#### 4.4 Instantaneous Nusselt and Sherwood numbers

The oscillations induced by the forcing functions suggest a variation in the values of the instantaneous Nusselt and Sherwood numbers. Equations 28 and 29 are used to calculate  $\text{Nu}_{\text{AVG}}$  and  $\text{Sh}_{\text{AVG}}$  along the length of the air/liquid-

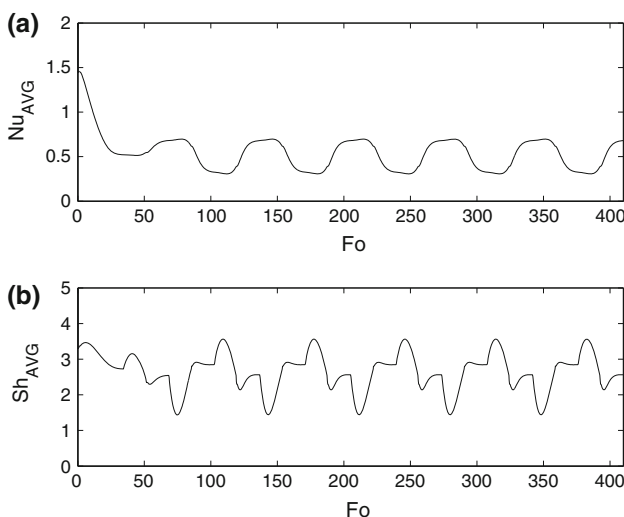


**Fig. 9** Instantaneous value of  $\text{Nu}_{\text{AVG}}$  and  $\text{Sh}_{\text{AVG}}$  for step changes in  $\zeta$  ( $\xi = 0$ ,  $\text{Fo}$ )

desiccant interface at every instant in time. Due to the strong changes observed in all the variables caused by steps changes in  $\zeta$  ( $\xi = 0$ ,  $\text{Fo}$ ), this case has been used for the analysis. Figure 9a and b show the variation of  $\text{Nu}_{\text{AVG}}$  and  $\text{Sh}_{\text{AVG}}$  over time, respectively. The instantaneous Nusselt number displays a smoother fluctuation compared to the instantaneous Sherwood number. The Nusselt number follows closely the variation seen in  $\theta_a$  in Fig. 8a and it reaches a minimum value of 0.30 and a maximum of 0.69 after the effect of the initial conditions.  $\text{Sh}_{\text{AVG}}$  oscillates between 1.43 and 3.56 with several maxima and minima that result from the combined effects of delay and variation in the amplitude of oscillations along the channel length.

$$\text{Nu}_{\text{AVG}} = \frac{4\delta_a}{H} \int_0^H \frac{1}{T_w^0 - T_a} \left. \frac{\partial T_a}{\partial y_a} \right|_{y_a=\delta_a} dx \quad (28)$$

$$\text{Sh}_{\text{AVG}} = \frac{4\delta_a}{H} \int_0^H \frac{1}{\omega_{\text{int}} - \omega^0} \left. \frac{\partial \omega}{\partial y_a} \right|_{y_a=\delta_a} dx \quad (29)$$

## 5 Conclusions

Liquid desiccant systems provide the benefit of reducing the latent loads in air conditioning systems with the benefit of increasing the coefficient of performance especially in humid climates. In this paper, a transient two dimensional model of the heat and mass transfer in parallel flow inside a channel is developed. The transient distribution of water content in the air and liquid desiccant were obtained and the effect of oscillatory behavior in the form of step changes of a single parameter were

studied. The instantaneous average Nusselt and Sherwood numbers along the air/liquid-desiccant interface are also presented.

**Acknowledgments** This work has been supported by the California Energy Commission and the California Institute for Energy and Environment contract number MR-07-04.

**Open Access** This article is distributed under the terms of the Creative Commons Attribution Noncommercial License which permits any noncommercial use, distribution, and reproduction in any medium, provided the original author(s) and source are credited.

## References

1. Armstrong PR, Brusewitz GH (1984) Design and testing of a liquid desiccant dehumidifier. *Trans ASAE* 27(1):169–172
2. Lowenstein A, Slayzak S, Kozubal E (2006) A zero carryover liquid-desiccant air conditioner for solar applications. In: Proceedings of the ASME international solar energy conference ISEC2006-99079, Denver, CO, pp 1–11
3. Park MS, Howell JR, Vliet GC, Peterson JL (1994) Coupled heat and mass transfer between a falling film and air in cross-flow. *Int J Heat Mass Transf* 37(1):395–402
4. Khan AY (1998) Cooling and dehumidification performance analysis of internally-cooled liquid desiccant absorbers. *Appl Therm Eng* 18(5):265–281
5. Kessling W, Laevemann E, Kapfhammer C (1998) Energy storage for desiccant cooling component development. *Sol Energy* 64(4–6):209–221
6. Rahamah A, Elsayed MM, Al-Najem NM (1998) A numerical solution for cooling and dehumidification of air by a falling desiccant film in parallel flow. *Renew Energy* 13(3):305–322
7. Ali A, Vafai K, Khaled A-RA (2003) Comparative study between parallel and counter flow configurations between air and falling film desiccant in the presence of nanoparticle suspensions. *Int J Energy Res* 27:725–745
8. Ali A, Vafai K, Khaled A-RA (2004) Analysis of heat and mass transfer between air and falling film in a cross flow configuration. *Int J Heat Mass Transf* 47:743–755
9. Ali A, Vafai K (2004) An investigation of heat and mass transfer between air and desiccant film in an inclined parallel and counter flow channels. *Int J Heat Mass Transf* 47:1745–1760
10. Mesquita LCS, Harrison SJ, Thomey D (2006) Modeling of heat and mass transfer in parallel plate liquid-desiccant dehumidifiers. *Sol Energy* 80:1475–1482
11. Chenqin R, Yi J, Guangfa T, Yianpin Z (2005) A characteristic study of liquid desiccant dehumidification/regeneration processes. *Sol Energy* 79:483–494
12. Ren CQ, Tu M, Wang HH (2007) An analytical model for heat and mass transfer processes in internally cooling or heated liquid desiccant-air contact units. *Int J Heat Mass Transf* 50:3545–3555
13. Liu X, Jiang Y, Xia J, Chang X (2007) Analytical solutions of coupled heat and mass transfer processes in liquid desiccant air dehumidifier/regenerator. *Energy Convers Manag* 48:2221–2232
14. Hajji A, Worek WM (1992) Transient heat and mass transfer in film absorption of finite depth with nonhomogeneous boundary conditions. *Int J Heat Mass Transf* 35(9):2101–2108
15. Nakoryakov VE, Bufetov NS, Grigorieva NI, Dekhtyar RA (2003) Heat and mass transfer during vapor absorption by a stagnant solution layer. *J Appl Mech Tech Phys* 44(2):236–242

16. Nakoryakov VE, Bufetov NS, Grigorieva NI, Dekhtyar RA, Marchuk IV (2004) Vapor absorption by immobile solution layer. *Int J Heat Mass Transf* 47:1525–1533
17. Gandhidasan P, Al-Farayedhi AA, Antar MA (2002) Investigation of heat and mass transfer in a gauze-type structured packing liquid desiccant dehumidifier. *Int J Energy Res* 26:1035–1044
18. Peng SW, Pan ZM (2009) Heat and mass transfer in liquid desiccant air-conditioning process at low flow conditions. *Commun Nonlinear Sci Numer Simulat* 14:3599–3607
19. Tauscher R, Dinglreiter U, Durst B, Mayinger F (1999) Transport processes in narrow channels with application to rotary exchangers. *Heat Mass Transf* 35:123–131
20. Al-Sharqawi HS, Lior N (2004) Conjugate computation of transient flow and heat and mass transfer between humid air and desiccant plates and channels. *Numerical Heat Transf Part A* 46:525–548
21. Yin J, Jensen MK (2003) Analytic model for transient heat exchanger response. *Int J Heat Mass Transf* 46:3255–3264
22. Ansari MR, Mortazavi V (2006) Simulation of dynamical response of a countercurrent heat exchanger to inlet temperature or mass flow rate change. *Appl Therm Eng* 26:2401–2408
23. Mishra M, Das PK, Sarangi S (2008) Effect of temperature and flow nonuniformity on transient behavior of crossflow heat exchanger. *Int J Heat Mass Transf* 51:2583–2592
24. Pineda SM, Diaz G (2009) Analysis of heat and mass transfer of an adiabatic cross-flow liquid desiccant absorber operating at low temperature. In: Proceedings of ASME summer heat transfer conference. Paper # HT2009-88255, San Francisco, pp 1–9